THE JOURNAL OF PHYSICAL CHEMISTRY B

Article

pubs.acs.org/JPCB

Dielectric Properties of Water Ice, the Ice Ih/XI Phase Transition, and an Assessment of Density Functional Theory

Mandes Schönherr,[†] Ben Slater,[‡] Jürg Hutter,[†] and Joost VandeVondele*[,§]

[†]Institute of Physical Chemistry, University of Zürich, Winterthurerstrasse 190, CH-8057 Zürich, Switzerland

[‡]Department of Chemistry, University College London, London WC1H 0AJ, England

[§]Department of Materials, ETH Zürich, Wolfgang-Pauli-Strasse 27, CH-8093 Zürich, Switzerland

ABSTRACT: The dielectric properties of the hydrogen disordered hexagonal phase (Ih) of water ice have been computed using density functional theory (DFT) based Monte Carlo simulations in the isobaric−isothermal ensemble. Temperature dependent data yield a fit for the Curie−Weiss law of the system and hence a prediction of the temperature of the phase transition from the Ih phase to the hydrogen ordered ice XI phase. Direct simulations around the phase transition temperature confirm and refine the predicted phase transition temperatures and provide data for further properties, such as the linear thermal expansion coefficient. Results have been obtained with both hybrid and semilocal density functionals, which yields insight in the performance of the electronic structure method. In particular, the hybrid functional yields significantly more realistic dielectric constants than the semilocal variant, namely $\varepsilon \approx 116$ as opposed to $\varepsilon \approx 151$ at 273 K ($\varepsilon_{\text{experiment}} = 95$). This can be attributed to the tendency of semilocal functionals to be biased to configurations with a large dipole moment, and their overestimation of the dipole moments of these configurations. This is also reflected in the estimates of the Ih/XI transition temperature, which is 70−80 and 90−100 K for the hybrid and semilocal functional respectively. DFT based sampling of the millions of configurations necessary for this work has been enabled by a Tree Monte Carlo algorithm, designed for massively parallel computers.

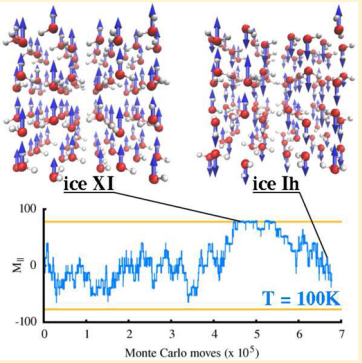

INTRODUCTION

Water ice is a ubiquitous substance and yet despite its familiarity and intensive study for centuries, some of its most basic properties are not fully understood. For example, in the 1850s, Michael Faraday proposed the surface of ice was "liquid-like",[1] yet a detailed atomic scale understanding of this structure is still elusive. Below the onset of "quasi-liquid layer" formation, ice at ambient temperature (ice Ih) is fully crystalline. However, although the water ice surface shows both short and long-range order, it also displays behavior normally associated with amorphous materials;[2] surface and subsurface vacancy formation energies, which would expected to be similar, vary by ≈0.8 eV, approximately 3 times the strength of a hydrogen bond. This observation is explicable through consideration of the effects of *orientational disorder*, where a water molecule can adopt one of six possible orientations; the orientational disorder leads to positional disorder of the hydrogen atoms on an ordered oxygen sublattice. This disorder contributes to the amazing richness in ice's phase diagram, giving rise to 15 known phases.[3] This hydrogen disorder is the result of a delicate balance between configurational entropy, which has been accurately estimated by Pauling[4] and Giauque,[5] and the small energy differences between the various configurations[6] that respect the Bernal−Fowler ice rules.[7] This disorder, and the associated fluctuations of the total dipole of the sample, lead to a high dielectric constant for solid water ice Ih (ε(272K) = 95), which is surprisingly similar to that of liquid water (ε(278K) = 86). The term "dielectric constant" of ice Ih is somewhat imprecise, as the hexagonal symmetry of ice Ih implies that the dielectric tensor will have two unique eigenvalues, $\varepsilon_{\perp}$ and $\varepsilon_{\parallel}$. The former value is 2-fold degenerate, with eigenvectors in the hexagonal plane and orthogonal to the optical axis (also named *c* or *z* axis), whereas the eigenvector corresponding to the latter is parallel to the optical axis of the crystal. Indeed, the dielectric anisotropy of ice is exploited in the characterization of polar ice sheets by radio waves[8] as polycrystalline ice causes a distinct attenuation of radio waves in comparison to oriented ice. If all microscopic configurations of ice are energetically equivalent, as assumed in the Pauling model (see also Minagawa[9]), the anisotropy $((\varepsilon_{\parallel} - \varepsilon_{\perp})/\varepsilon_{\parallel})$ is found to be vanishingly small (see, e.g., Aragones et al.[10]). Early measurements of this anisotropy, performed by Paul Scherrer and co-workers in a freezer room of a local brewery in Zurich,[11] yield an anisotropy of 13% near the melting temperature. This value, later confirmed (12%) and extended to a wider temperature range by Kawada,[12] suggests that the precise energetics of these configurations does matter and that the Pauling model is thus not sufficient in this context. The trigger for these experiments at low temperature was his earlier observation[13] of an indication for a phase transition near 70 K to what is now known as the proton ordered, ferroelectric, hexagonal phase ice XI.[14] Such a phase transition should be

Received: October 18, 2013
Revised: December 17, 2013
Published: December 18, 2013

clearly visible in the dielectric properties, as the ordered phase has a low dielectric constant, whereas the relevant component of the dielectric tensor of the high temperature phase can be approximated by a Curie−Weiss law

$$\varepsilon_{\parallel} - \varepsilon_{\infty} = A/(T - T_C) \quad (1)$$

where A is the Curie constant and T_C is the Curie temperature, which should be similar to the phase transition temperature. These experiments are challenging and have led to a wide range (6−127 K) of estimates for T_C, as reviewed in ref 15. The origin of this difficulty is the long dielectric relaxation time in pure ice and the slow kinetics of the phase transition, which requires doping with KOH to reduce the associated time constants from years to more manageable values. The uncertain influence of the dopant and the difficulty of growing single crystals containing KOH have made characterization of this phase transition a challenge to experiment. Nevertheless, recent dielectric experiments agree on a phase transition temperature of 72 K for H_2O[16,17] (76 K for D_2O[14]), whereas thermally stimulated depolarization provides further evidence for ferroelectric ordering,[18] and neutron diffraction has provided the crystal symmetry ($Cmc2_1$) of the ice XI phase.[19,20] The dielectric tensor should thus be considered a quantity that is very sensitive to important aspects of water, namely the polarization of the system, and the detailed energetics of the various hydrogen bonding configurations. The fact that the structure of ice Ih, contrary to that of the liquid (see ref 21 for a recent discussion), is well-known, also makes the system ideal to quantitatively assess the quality of simulation models. Furthermore, simulation models that reproduce the well established experimental data, for example the high temperature dielectric tensor, can than be used to investigate more controversial aspects, such as the influence of electrostatic screening between charged defects and orientational (Bjerrum) defects. It is important to recognize that force-field based approaches, including sophisticated high order multipole models cannot currently accurately capture subtle differences in energy between hydrogen orderings. Therefore, quantum mechanical based approaches are essential for benchmarking. Nevertheless, force field based approaches have provided tremendously instructive insights into ice physics. Rick and Haymet proposed a Monte Carlo move suitable for off-lattice calculations of ice[22] and demonstrated that several non-polarizable empirical atomistic models of water significantly underestimate (by 100%) the dielectric constant of ice. This result was later verified and extended by several other groups.[10,23,24] Adding polarizability to the model improved results significantly, which was attributed to the larger molecular dipole in these models.[22] However, none of the methods displayed a significant anisotropy of the dielectric tensor, as observed experimentally, which may relate to the fact that these models predict an antiferroelectric ordered phase to be more stable than the experimental ferroelectric phase.[10,22,24] In fact, Hirsch and Ojamäe found[6] an almost anticorrelation between the energies computed with density functional theory (DFT) and empirical methods for the 16 unique proton-ordered configurations compatible with an orthorhombic unit cell containing eight water molecules, which has been attributed to incorrect higher order electrostatic multipoles in the empirical force fields.[25] Furthermore, HF and DFT yield (independent of the density functional employed), a lowest energy configuration that is indeed ferroelectric,[6,25−28] indicating that these methods might be capable of reproducing the fine energy details in this system. Singer and co-workers parametrized an analytical model based on graphs, i.e., hydrogen bond network patterns, to DFT (BLYP) reference values, and with this approach were able to perform Monte Carlo simulations that predict the phase transition temperature between Ih and XI to be 98 K in good agreement with experiment.[26,29] This is a very interesting and powerful approach but is probably limited to models containing less than ≈60−70 molecules, because of the combinatorial explosion of enumerating possible hydrogen bonding arrangements. In addition, the model may not be easily extended to consider orientational (Bjerrum) or ionic defects (i.e., hydronium and hydroxide). Unfortunately, the dielectric properties were not reported, so cross validating the employed model directly is not possible. In all simulations discussed here, nuclear quantum effects, which are relatively small in this context, have not been taken into account, and hence comparison with results for D_2O, which is the more "classical" isotope, will be considered whenever possible. Rusnak and co-workers estimated the static dielectric constants of liquid water and ice for PBE, using a free energy perturbation approach that employs a classical potential to sample configurations, which are reweighted to ab initio values.[30] However, obtained results underestimate the experimental value significantly (ε(253K) = 67). This difference might in part be due to their use of a Bader-like analysis to obtain molecular dipoles, instead of relying on the modern theory of polarization.[31,32] The latter theory was employed in the simulations of Sharma et al. to compute the dielectric constant of liquid water.[33] Based on a 20 ps simulation of liquid water with the PBE functional in the canonical ensemble (NVT), a value in surprisingly good agreement with experiment was obtained (ε(330K) = 67 vs ε(330K) = 68). For ice Ih, the proton configurations could not be sampled, but a molecular dipole derived from a representative ice configuration (3.32 D), in good agreement with experiment would be obtained for a plausible angular correlation factor $G_K \approx 2.55$. It is noteworthy that the same correlation factor obtained by commonly used empirical potentials varies in the range 1.34−2.7.[10]

In the current work, the merits of the various approaches mentioned above have been combined, and explicit sampling of hydrogen disorder at the DFT level is employed (1) to compute the dielectric tensor at various temperatures using the modern theory of polarization, (2) to determine the Ih/XI phase transformation temperature directly, and (3) to assess the quality of semilocal and hybrid density functional theory for water ice.

■ COMPUTATIONAL METHODS

Calculations have been performed with the free simulation package CP2K/Quickstep[34,35] that has been enhanced with a Monte Carlo (MC) algorithm, named Tree Monte Carlo (TMC). The system studied consists of 96 water molecules in an orthorhombic cell, initially 13.57 Å × 15.67 Å × 14.73 Å. This cell is sufficiently large to allow for a Gamma-point calculations and is similar in size to the classical model systems employed previously (e.g., 128 molecules in ref 22). Near the phase transition temperature, size effects cannot be excluded. Monte Carlo simulations have been performed in the isobaric−isothermal (NPT) ensemble[36] at 1 bar, except when the canonical (NVT) ensemble is mentioned explicitly. DFT calculations are based on the semilocal functionals by Perdew, Burke, and Ernzerhof (PBE)[37] and by Becke, Lee, Yang, and

dx.doi.org/10.1021/jp4103355 | J. Phys. Chem. B 2014, 118, 590−596

Parr (BLYP)[38,39] and the corresponding hybrid functionals PBE0[40] and B3LYP.[39,41,42] The latter two functionals contain a fraction of Hartree−Fock exchange (denoted HFX), 25% and 20%, respectively, and are thus nonlocal. All functionals are combined with a dispersion correction by Grimme (which we denote D2),[43] which is essential to obtain a qualitatively correct density of liquid water in *NPT* simulations.[44] Norm-conserving Goedecker−Teter−Hutter (GTH)[45] pseudopotentials are employed together with a triple-ζ valence basis set and two polarization functions (TZV2P). HFX is computed with a robust γ-point implementation[46,47] using a truncation radius of 6 Å, and the auxiliary density matrix method (ADMM) with the pFIT3 basis.[48] Periodic boundary conditions have been used throughout, and electrostatics are computed using an Ewald-sum. This implies so-called conducting or tinfoil boundary conditions,[49] suitable for samples embedded in a medium of high dielectric constant, and is equivalent to enforcing closed circuit electrical boundary conditions without applied bias.[50] These boundary conditions are almost always applied in electronic structure calculations and typically used in force field based simulation of ice (see, e.g., refs 10, 22, and 24). The plane wave cutoff was 800 Ry for *NPT* and 400 Ry for *NVT* calculations, with the number of grid points kept fixed during *NPT* simulations.[35,51]

The elements of the dielectric tensor are obtained as the second moments of the dipole distribution using

$$\varepsilon_{\alpha\beta} = \varepsilon_\infty + \left(\frac{4\pi}{3Vk_BT}\right)(\langle M_\alpha \cdot M_\beta\rangle - \langle M_\alpha\rangle\langle M_\beta\rangle) \quad (2)$$

where M_α is the component of the total cell dipole in the α direction, ε_∞ is the optical dielectric constant, taken to be 1 in the following, and $\langle\cdot\rangle$ denotes ensemble averaging. In the context of periodic DFT, changes in the cell dipole are obtained from the Berry phase formulation of polarization.[31]

Monte Carlo generates a sequence of configurations, a Markov chain, that samples a given ensemble based on acceptance/rejection of random configurational changes (moves). Three important strengths of Monte Carlo are exploited in the context of this study. First, in addition to the traditional moves (atom and molecule translation, molecule rotation, and nonisotropic volume changes), a proton reordering move is employed.[22] This specialized move allows for reorienting several molecules in a closed loop of hydrogen bonded neighbors in a way that obeys the Bernal−Fowler ice rules and may change the effective dipole of the unit cell, circumventing the high energy barriers that the physical process must overcome in experiment or unbiased molecular dynamics simulations. Second, in the context of DFT it is advantageous to employ a presampling strategy in which a sub-Markov chain is generated with an approximate classical potential.[51−53] In this nested MC approach, the entire sub-Markov chain is accepted/rejected with a single DFT calculation, leading to exact sampling of the DFT potential at much reduced computational cost. Note that converged MC results are independent of the approximate classical potential, but the rate of convergence depends on the quality of the approximation. Here a refitted classical nonpolarizable potential based on the model from ref 54 has been employed, which provides good acceptance. In our current approach, 50 (*NPT*) or 100 (*NVT*) nested MC moves are applied, which are constrained to a fixed subcell with edges of length 8 Å to retain sufficiently large acceptance rates in the DFT step. This nested MC setup leads to a high fraction of the DFT calculations being employed to accept/reject hydrogen reordering moves, resulting in effective sampling of the cell dipole. Third, Monte Carlo contains an intrinsic parallelism that has so far not yet been exploited in molecular simulation but is here used by the TMC algorithm for obtaining long Markov chains on massively parallel computers. It is based on the observation that new (future) configurations in the Markov chain can be constructed on the fly and instantaneously, before the energy of the current configuration has been evaluated, as neither energy nor forces are required for the MC moves.[55] This approach requires speculation on the outcome of the acceptance check or, when used in a systematic fashion, builds a tree of configurations assuming both possible outcomes of this check. All the configurations present in the tree can be computed simultaneously, limited only by the available resources. Finally, the Markov chain, identical to the conventional serial one, is constructed, discarding the configurations that are off the chain, as the energies become available. The implementation of this algorithm, which includes a number of techniques to reduce the amount of discarded work, is freely available[34] and will be discussed in more detail elsewhere. TMC has been key to reduce the wall time per generated Markov chain element to 2.5 and 14 s for PBE and PBE0 respectively, and ultimately allowed for single MC chains with nearly a million moves.

RESULTS AND DISCUSSION

The temperature dependent dielectric constant of ice Ih at ambient pressure is a central result of this work. It is a challenging quantity to obtain by simulation, as extensive sampling is necessary for convergence. However, provided 100000s of MC steps are performed, convergence can be reached even with first principles simulations. This is demonstrated for five MC simulations in the *NPT* ensemble, based on either the PBE-D2 or PBE0-D2 functional, in the upper panel of Figure 1. The relevant components of the dielectric tensor obtained by these simulations are summarized in Table 1. These data clearly show that ε obtained with PBE-D2 is significantly larger than the one obtained with PBE0-D2. At the melting point, $\varepsilon(273\text{K}) = 116$ is in fair agreement with the experimental result of Johari et al.[15] $\varepsilon(273\text{K}) = 95$, whereas PBE-D2 significantly overestimates it ($\varepsilon(273\text{K}) = 151$). The origin of this difference is related to the nature of the density functionals, as we discuss in more detail below. Of particular interest is the value of the dielectric anisotropy $((\varepsilon_\parallel - \varepsilon_\perp)/\varepsilon_\parallel)$, because it is indicative of the XI/Ih phase transition. Simulations based on empirical force fields predict very small or zero values of the anisotropy.[10,22,24] PBE0-D2 calculations at 273 K result in an anisotropy value of 18%, which is slightly greater than the measured value of approximately 12% of Kawada et al.[12] PBE-D2 overestimates the anisotropy more significantly (22%), indicative of a bias toward configurations that display a large dipole along the parallel direction. Note that, the average *molecular* dipole moments found for apolar ice slabs computed with PBE were approximately 10% greater than PBE0,[2] which contributes to the observed difference in anisotropy using the semilocal and hybrid functionls. As the temperature decreases and the Ih/XI phase transition temperature approaches, the anisotropy becomes larger. A fit of the Curie−Weiss law through the simulation data, shown in the lower panel of Figure 1 yields $T_C = 60$ K and $T_C = 79$ K for PBE0-D2 and PBE-D2, respectively. However, given the limited data, the uncertainty in this fit is likely large, on the order of 10

dx.doi.org/10.1021/jp4103355 | J. Phys. Chem. B 2014, 118, 590−596

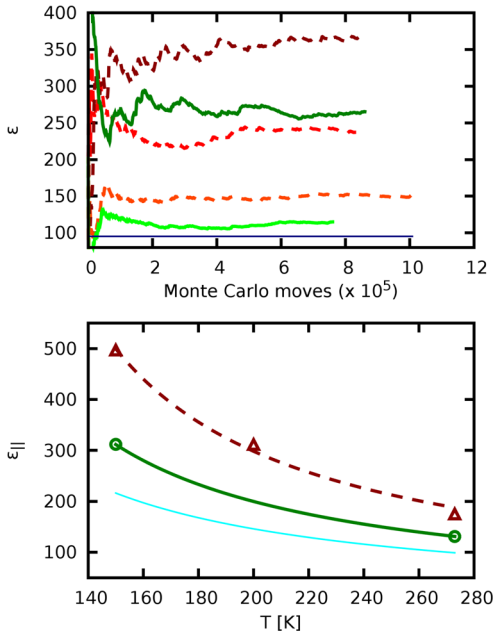

Figure 1. Upper panel: running averages of ε for PBE-D2 at 273 K (orange), 200 K (red), and 150 K (brown) and PBE0-D2 at 273 K (light green) and 150 K (green). The experimental value of Johari[15] at 273 K is shown in blue. Lower panel: converged values of $\varepsilon_\perp$ for PBE0-D2 (circles) and PBE-D2 (triangles), with the corresponding fit (solid green and dashed brown lines) of Curie–Weiss law (1). Experimental data of Kawada et al.[16] (light blue) are shown for comparison.

Table 1. Elements of the Dielectric Tensor and Dielectric Anisotropy Obtained with PBE-D2 and PBE0-D2 in the *NPT* Ensemble[a]

	T (K)	10^5 MC moves	ε	$\varepsilon_\perp$	$\varepsilon_\parallel$	$(\varepsilon_\parallel - \varepsilon_\perp)/\varepsilon_\parallel$
PBE0-D2	273	7.6	116	108 ± 3	131	17%
PBE0-D2	150	8.6	266	234 ± 0	331	30%
PBE-D2	273	10.1	151	139 ± 7	174	20%
PBE-D2	200	8.3	238	202 ± 7	310	35%
PBE-D2	150	8.4	366	298 ± 28	502	41%

[a]The difference between ε_{xx}, ε_{yy}, and $\varepsilon_\perp = (\varepsilon_{xx} + \varepsilon\varepsilon_{yy})/2$ is used as an estimate of the statistical uncertainty.

K. Furthermore, a true divergence as described by equation eq 1 cannot be observed due to finite size effects. Nevertheless, the Curie temperatures found are close to the experimental phase transition temperature; 72 K for H_2O and 76 K for D_2O.

On the basis of these estimates, the phase transition temperature has been determined by direct simulation. In particular, *NPT* MC runs at various temperatures between 50 and 100 K have been started from the same ice Ih configuration and run for at least 250 000 MC steps. As shown in Figure 2, this leads to a spontaneous phase transformation to the expected ice XI phase for the low temperatures, whereas the systems at the higher temperatures remain in the ice Ih phase. The resulting phase transition temperatures can thus be bracketed by 70–80 K (PBE0-D2) and 90–100 K (PBE-D2), in fair agreement with the estimates derived from the Curie–Weiss fit. The PBE-D2 result is in agreement with the 98 K computed by a graph based model parametrized to the semilocal BLYP functional, yielding additional support for this approach.[26,29] Nevertheless, the PBE0-D2 model can be assumed to be the most predictive, given its favorable

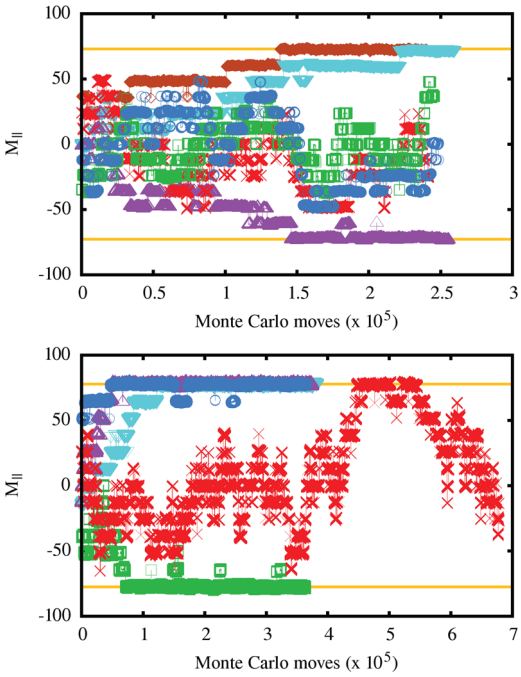

Figure 2. Evolution of the z component of the total cell dipole for *NPT* calculations at various temperatures: upper panel, PBE0-D2; lower panel, PBE-D2. The different colors and symbols correspond to 100 K (red, crosses), 90 K (green, squares), 80 K (blue, circles), 70 K (violent, triangles up), 60 K (light blue, triangles down), and 50 K (brown, diamonds). The solid (orange) lines indicate the permanent dipole of the ice XI phase.

comparison to dielectric experimental data, obtained with well established experiments near the melting point. Furthermore, the fact that the transition temperature is relatively insensitive to the precise DFT model suggests that this prediction will be robust.

The advantage of direct MC simulation of a reliable atomistic model is that further properties can be obtained from the generated trajectories. Here we investigate the temperature dependent density, or equivalently the volume, given its relevance for ε (see below) and the fact that this quantity is directly accessible from the *NPT* simulations performed. Indeed, *NPT* simulations employ a flexible simulation cell, which fluctuates around a temperature dependent average value (σ(273K) ≈ 0.12 Å for our simulation cell). At the melting point, both models overestimate the density, with 0.960 and 0.995 g/cm^3 for PBE0-D2 and PBE-D2 respectively, compared to the experimental results obtained by Röttger[56] (0.917 g/cm^3). PBE0-D2 is again the best model, with a volume that is underestimated by 4.5%. The temperature dependence of the volume can be described by the linear thermal expansion coefficient $\alpha(T)$ defined by

$$\alpha(T) = \frac{1}{3}\frac{1}{V(T)}\frac{\partial V(T)}{\partial T} \quad (3)$$

Only for PBE-D2 are sufficient data available to yield a stable polynomial fit of the temperature dependence of the volume, using a third-order polynomial for the ice Ih phase (100–273 K) and a second-order polynomial for the ice XI phase (60–90 K). In Figure 3, the corresponding $\alpha(T)$ is compared to the experimental results by Röttger.[56] Given the slow kinetics of the XI/Ih phase transition, it is reasonable to assume that the

dx.doi.org/10.1021/jp4103355 | J. Phys. Chem. B 2014, 118, 590–596

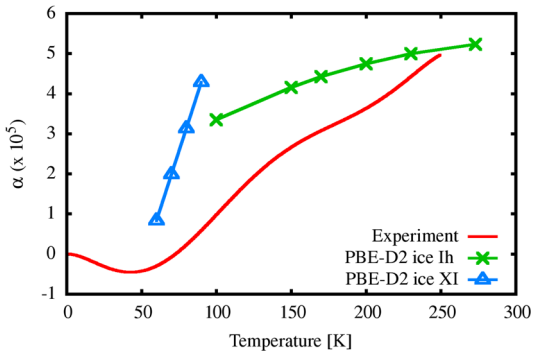

Figure 3. Linear expansion coefficient α, fitted using *NPT* ensembles calculated with and PBE-D2 functionals for the ice Ih phase (crosses) and ice XI phase (triangles), compared with experimental results of D_2O of Röttger[56] (solid red line).

experimental system consists of a mixture of both phases,[57] with a precise constitution that depends on the preparation method. Indeed, ice XI has never ever been reported to have been made more than 70% pure.[14] It is therefore reasonable to assume that the experimental curve can be approximated by a combination of the simulation data of the pure phases, which suggests good qualitative agreement. In particular, for even lower temperatures, a negative thermal expansion coefficient could be expected.

Finally, we show that the observed differences between PBE-D2 and PBE0-D2 are more general in nature. To do so, we have performed MC simulations at constant volume (*NVT*), 273 K, and experimental density, and compared two pure DFT (PBE-D2 and BLYP-D2) and two hybrid (B3LYP-D2 and PBE0-D2) functionals. The data for these simulations is summarized in Table 2. Constant volume simulations facilitate

Table 2. Elements of the Dielectric Tensor and the Dielectric Anisotropy Obtained in the *NVT* Ensemble at 273 K and Experimental Density with the PBE-D2, PBE0-D2, BLYP-D2, and B3LYP-D2 Functionals[a]

	T (K)	10^5 MC moves	ε	$\varepsilon_\perp \pm ((\varepsilon_{xx}-\varepsilon_{yy})/2)$	$\varepsilon_\parallel$	$(\varepsilon_\parallel-\varepsilon_\perp)/\varepsilon_\parallel$
exp (ref 15)	273		95			
exp (ref 12)	273		90	87	99	12%
PBE-D2	273	6.9	127	114 ± 2	152	25%
PBE-D2 (106%)	273	3.2	145	126 ± 3	183	31%
PBE0-D2	273	2.8	103	98 ± 4	112	12%
BLYP-D2	273	13.7	122	110 ± 1	144	24%
B3LYP-D2	273	3.2	110	98 ± 1	133	26%

[a]To illustrate the effect of compression, one additional *NVT* result at 106% of the density is provided for PBE-D2.

the comparison between the functionals and can be used to highlight the importance of employing the *NPT* ensemble for the calculation of the dielectric constant. In particular, the PBE-D2 simulations have been performed at 100% and 106% of the experimental density, the latter being similar to the equilibrium density of the PBE-D2 functional. Although the latter simulation yields ε = 145, very similar to the *NPT* results of ε = 151, the simulation at experimental density yields ε = 127, a significant reduction of the value. Compared to the *NPT* simulations, a similar reduction is also observed for PBE0-D2, which at experimental density provides an even better estimate of ε (103) and anisotropy (12%). This sensitivity of ε to the density (volume), suggests that modifications to the functional that improve the lattice parameters could yield enhanced dielectric properties. At the same density, the overestimation of ε in the case of semilocal functionals is due to two effects, visible in Figure 4. These effects are more important than the

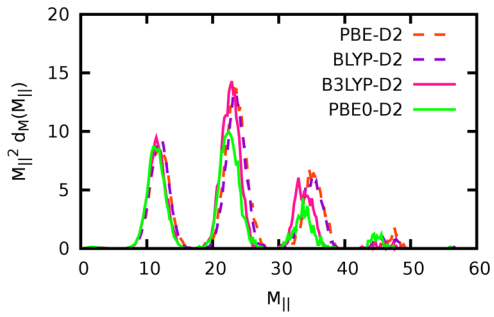

Figure 4. Distribution of the z component of the dipole moment, weighted by the dipole squared. This weighting corresponds to the contribution of these peaks to ε. Results have been computed for semilocal (PBE-D2 and BLYP-D2) and hybrid (B3LYP-D2 and PBE0-D2) functionals in the *NVT* ensemble at 273 K.

small differences in geometry between semilocal and hybrid functionals (e.g., r_{OH} = 1.000 and r_{OH} = 0.985, respectively). First, as can be seen as a shift of the position of the peaks, dipoles of a given configuration are enhanced by roughly 5%. Second, visible by the area under the peaks, these polarized configurations are sampled more often, i.e., are energetically favorable. Both effects are consistent with the overestimation of polarizability by semilocal density functionals (see also ref 2) and with the improvements expected for a hybrid functional.[58] Ultimately, this is a result of the underestimation of the band gap by semilocal functionals, a deficiency that is, also in water ice, significantly improved by hybrid functionals.[28]

CONCLUSION

The temperature dependent dielectric constant of ice Ih contains a wealth of information about the interactions between water molecules. It contains the most visible signature of the Ih/XI phase transition, which is the result of a delicate balance between energy and entropy. Here, this property has been computed directly from extensive sampling of hybrid and semilocal DFT models in the appropriate ensemble. We find that semilocal DFT significantly overestimates the dielectric constant (ε(273K) ≈ 150 for PBE-D2), whereas hybrid density functionals (ε(273K) ≈ 116 for PBE0-D2) provide better agreement with experiment (ε(273K) ≈ 95). The electronic overpolarization and the energetic bias toward configurations with large dipole both contribute to the error observed for the semilocal functional. This effect is also observed for a different family of functionals (BLYP-D2 and B3LYP-D2) and is thus likely of general nature. Furthermore, we expect that this error will also be present in the liquid phase, which could have implications, for example, for simulations of the behavior of water near (electrified) interfaces, or for the solvation and interaction of ions including incipient species such as the Zundel ion and processes involving proton transport. The Ih/XI phase transition temperature has been determined both from a Curie–Weiss fit and from direct MC simulations for both PBE0-D2 and PBE-D2. All these values are in good agreement, lending support to our methodology, and yield a

dx.doi.org/10.1021/jp4103355 | J. Phys. Chem. B 2014, 118, 590–596

transition temperature of 70−80 K (PBE0-D2) or 90−100 K (PBE-D2). Given the validation of our model via the dielectric constant, we expect the PBE0-D2 model to be most predictive. This PBE0-D2 result confirms accurately the measurements by Kawada (ref 16) and thus suggests that the experimental procedure of KOH doping can indeed be used to accelerate the kinetics of the Ih/XI phase transformation without influencing the final equilibrium structure formed. Finally, MC sampling of explicit atomistic models yields data that can be used to compute several properties, and as an example, the linear thermal expansive coefficients of ice Ih and XI has been reported in their respective temperature ranges. This shows that the steady increase in computer power and the development of novel algorithms have made the extensive sampling of disordered solids at the DFT level possible, and that this approach can now be used to evaluate properties that have long challenged experiment and theory alike.

AUTHOR INFORMATION

Corresponding Author

*J. VandeVondele: e-mail, Joost.VandeVondele@mat.ethz.ch.

Notes

The authors declare no competing financial interest.

ACKNOWLEDGMENTS

The authors acknowledge useful comments on the manuscript from Christoph Salzmann. J.V. acknowledges financial support by the European Union FP7 in the form of an ERC Starting Grant under contract no. 277910. Preliminary calculations were performed using resources of the National Center for Computational Sciences at Oak Ridge National Laboratory (ORNL), which is supported by the Office of Science of the U.S. DOE under Contract No. DE-AC05-00OR22725, enabled by a 2011 INCITE award. Further calculations were enabled by a grant of the Swiss National Supercomputer Centre (CSCS) under project IDs s281, s441, and h05. The research leading to these results has received funding from the Swiss University Conference through the High Performance and High Productivity Computing (HP2C) Programme.

REFERENCES

(1) Faraday, M. On Certain Conditions of Freezing Water. *Athemaeum* **1850**, *1181*, 640−641.
(2) Watkins, M. B.; Pan, D.; Wang, E. G.; Michaelides, A.; VandeVondele, J.; Slater, B. Large Variation of Vacancy Formation Energies in the Surface of Crystalline Ice. *Nat. Mater.* **2011**, *10*, 794−798.
(3) Salzmann, C. G.; Radaelli, P.; Slater, B.; Finney, J. The Polymorphism of Ice: Five Unresolved Questions. *Phys. Chem. Chem. Phys.* **2011**, *13*, 18468−18480.
(4) Pauling, L. The Structure and Entropy of Ice and of Other Crystals with some Randomness of Atomic Arrangement. *J. Am. Chem. Soc.* **1935**, *57*, 2680−2684.
(5) Giauque, W. F.; Stout, J. W. The Entropy of Water and the Third Law of Thermodynamics. The Heat Capacity of Ice from 15 to 273 K. *J. Am. Chem. Soc.* **1936**, *58*, 1144−1150.
(6) Hirsch, T. K.; Ojamäe, L. Quantum-Chemical and Force-Field Investigations of Ice Ih: Computation of Proton-Ordered Structures and Prediction of Their Lattice Energies. *J. Phys. Chem. B* **2004**, 15856−15864.
(7) Bernal, J. D.; Fowler, R. H. A Theory of Water and Ionic Solution, with Particular Reference to Hydrogen and Hydroxyl Ions. *J. Chem. Phys.* **1933**, *1*, 515−548.
(8) Johari, G.; Jones, S. The Orientation Polarization in Hexagonal Ice Parallel and Perpendicular to the c-Axis. *J. Glaciol.* **1978**, *21*, 259−276.
(9) Minagawa, I. Ferroelectric Phase Transition and Anisotropy of Dielectric Constant in Ice Ih. *J. Phys. Soc. Jpn.* **1981**, *50*, 3669−3676.
(10) Aragones, J. L.; MacDowell, L. G.; Vega, C. Dielectric Constant of Ices and Water: A Lesson about Water Interactions. *J. Phys. Chem. A* **2011**, *115*, 5745−5758.
(11) Humbel, F.; Jona, F.; Scherrer, P. Anisotropie der Dielektrizitätskonstante des Eises. *Helv. Phys. Acta* **1953**, *26*, 17−32.
(12) Kawada, S. Dielectric Anisotropy in Ice Ih. *J. Phys. Soc. Jpn.* **1978**, *44*, 1881−1886.
(13) Kawada, S. Dielectric Dispersion and Phase Transition of KOH Doped Ice. *J. Phys. Soc. Jpn.* **1972**, *32*, 1442.
(14) Tajima, Y.; Matsuo, T.; Suga, H. Phase Transition in KOH-doped Hexagonal Ice. *Nature* **1982**, *299*, 810−812.
(15) Johari, G. P.; Whalley, E. The Dielectric Properties of Ice Ih in the Range 272−133 K. *J. Chem. Phys.* **1981**, *75*, 1333−1340.
(16) Kawada, S. Acceleration Of Dielectric Relaxation by KOH-Doping And Phase Transition In Ice Ih. *J. Phys. Chem. Solids* **1989**, *50*, 1177−1184.
(17) Oguro, M.; Whitworth, R. Dielectric Observations of the Transformation of Single Crystals of KOH-Doped Ice Ih to Ice XI. *J. Phys. Chem. Solids* **1991**, *52*, 401−403.
(18) Jackson, S. M.; Whitworth, R. W. Evidence for Ferroelectric Ordering of Ice Ih. *J. Chem. Phys.* **1995**, *103*, 7647−7648.
(19) Jackson, S.; Nield, V. Single-Crystal Neutron Diffraction Studies of the Structure of Ice XI. *J. Phys. Chem. B* **1997**, *5647*, 6142−6145.
(20) Leadbetter, R. C.; Ward, A. J.; Clark, J. W.; Tucker, P. A.; Matsuo, T.; Suga, H. The Equilibrium Low-Temperature Structure of Ice. *J. Chem. Phys.* **1985**, *82*, 424−428.
(21) Skinner, L. B.; Huang, C.; Schlesinger, D.; Pettersson, L. G. M.; Nilsson, A.; Benmore, C. J. Benchmark Oxygen-Oxygen Pair-Distribution Function of Ambient Water from X-Ray Diffraction Measurements with a Wide Q-Range. *J. Chem. Phys.* **2013**, *138*, 74506.
(22) Rick, S. W.; Haymet, A. D. J. Dielectric Constant and Proton Order and Disorder in Ice Ih: Monte Carlo Computer Simulations. *J. Chem. Phys.* **2003**, *118*, 9291−9296.
(23) Lindberg, G. E.; Wang, F. Efficient Sampling of Ice Structures by Electrostatic Switching. *J. Phys. Chem. B* **2008**, *112*, 6436−6441.
(24) MacDowell, L. G.; Vega, C. Dielectric Constant of Ice Ih and Ice V: A Computer Simulation Study. *J. Phys. Chem. B* **2010**, *114*, 6089−6098.
(25) Tribello, G. A.; Slater, B. Proton Ordering Energetics in Ice Phases. *Chem. Phys. Lett.* **2006**, *425*, 246−250.
(26) Singer, S. J.; Kuo, J.-L.; Hirsch, T. K.; Knight, C.; Ojamäe, L.; Klein, M. L. Hydrogen-Bond Topology and the Ice VII/VIII and Ice Ih/XI Proton-Ordering Phase Transitions. *Phys. Rev. Lett.* **2005**, *94*, 135701.
(27) Casassa, S.; Calatayud, M.; Doll, K.; Minot, C.; Pisani, C. Proton Ordered Cubic and Hexagonal Periodic Models of Ordinary Ice. *Chem. Phys. Lett.* **2005**, *409*, 110−117.
(28) Labat, F.; Pouchan, C.; Adamo, C.; Scuseria, G. E. Role of Nonlocal Exchange in Molecular Crystals: The Case of Two Proton-ordered Phases of Ice. *J. Comput. Chem.* **2011**, *32*, 2177−2185.
(29) Knight, C.; Singer, S. J.; Kuo, J.-L.; Hirsch, T. K.; Ojamäe, L.; Klein, M. L. Hydrogen Bond Topology and the Ice VII/VIII and Ih/XI Proton Ordering Phase Transitions. *Phys. Rev. E* **2006**, *73*, 1−14.
(30) Rusnak, A. J.; Pinnick, E. R.; Calderon, C. E.; Wang, F. Static Dielectric Constants and Molecular Dipole Distributions of Liquid Water and Ice-Ih Investigated by the PAW-PBE Exchange-Correlation Functional. *J. Chem. Phys.* **2012**, *137*, 034510.
(31) King-Smith, R.; Vanderbilt, D. Theory of Polarization of Crystalline Solids. *Phys. Rev. B* **1993**, *47*, 1651−1654.
(32) Spaldin, N. A. A Beginner's Guide to the Modern Theory of Polarization. *J. Solid State Chem.* **2012**, *195*, 2−10.
(33) Sharma, M.; Resta, R.; Car, R. Dipolar Correlations and the Dielectric Permittivity of Water. *Phys. Rev. Lett.* **2007**, *98*, 247401.

(34) The CP2K developer group, CP2K is freely available from http://www.cp2k.org/, 2013.
(35) VandeVondele, J.; Krack, M.; Mohamed, F.; Parrinello, M.; Chassaing, T.; Hutter, J. Fast and Accurate Density Functional Calculations Using a Mixed Gaussian and Plane Waves Approach. *Comput. Phys. Commun.* **2005**, *167*, 103−128.
(36) McDonald, I. NpT-Ensemble Monte Carlo Calculations for Binary Liquid Mixtures. *Mol. Phys.* **1972**, *23*, 41−58.
(37) Perdew, J.; Burke, K.; Ernzerhof, M. Generalized Gradient Approximation Made Simple. *Phys. Rev. Lett.* **1996**, *77*, 3865−3868.
(38) Becke, A. Density-Functional Exchange-Energy Approximation with Correct Asymptotic Behavior. *Phys. Rev. A* **1988**, *38*, 3098−3100.
(39) Lee, C.; Yang, W.; Parr, R. G. Development of the Colle-Salvetti Correlation-Energy Formula into a Function of the Electron Density. *Phys. Rev. B* **1988**, *37*, 785−789.
(40) Adamo, C.; Barone, V. Toward Reliable Density Functional Methods without Adjustable Parameters: The PBE0Model. *J. Chem. Phys.* **1999**, *110*, 6158−6170.
(41) Becke, A. D. Density-Functional Thermochemistry. III. The Role of Exact Exchange. *J. Chem. Phys.* **1993**, *98*, 5648−5652.
(42) Vosko, S. H.; Wilk, L.; Nusair, M. Accurate Spin-Dependent Electron Liquid Correlation Energies for Local Spin Density Calculations: A Critical Analysis. *Can. J. Phys.* **1980**, *58*, 1200−1211.
(43) Grimme, S. Semiempirical GGA-Type Density Functional Constructed with a Long-Range Dispersion Correction. *J. Comput. Chem.* **2006**, *27*, 1787−1799.
(44) Schmidt, J.; VandeVondele, J.; Kuo, I.-F. W.; Sebastiani, D.; Siepmann, J. I.; Hutter, J.; Mundy, C. J. Isobaric-Isothermal Molecular Dynamics Simulations Utilizing Density Functional Theory: An Assessment of the Structure and Density of Water at Near-Ambient Conditions. *J. Phys. Chem. B* **2009**, *113*, 11959−64.
(45) Goedecker, S.; Teter, M.; Hutter, J. Seperable Dual-Space Gaussian Pseudopotentials. *Phys. Rev. B* **1996**, *54*, 1703−1710.
(46) Guidon, M.; Schiffmann, F.; Hutter, J.; VandeVondele, J. Ab Initio Molecular Dynamics Using Hybrid Density Functionals. *J. Chem. Phys.* **2008**, *128*, 214104.
(47) Guidon, M.; Hutter, J.; VandeVondele, J. Robust Periodic Hartree-Fock Exchange for Large-Scale Simulations Using Gaussian Basis Sets. *J. Chem. Theory Comput.* **2009**, *5*, 3010−3021.
(48) Guidon, M.; Hutter, J.; VandeVondele, J. Auxiliary Density Matrix Methods for Hartree-Fock Exchange Calculations. *J. Chem. Theory Comput.* **2010**, *6*, 2348−2364.
(49) De Leeuw, S.; Perram, J.; Smith, E. Simulation of Electrostatic Systems in Periodic Boundary Conditions. I. Lattice Sums and Dielectric Constants. *Proc. R. Soc. Lond. A* **1980**, *373*, 27−56.
(50) Stengel, M.; Spaldin, N.; Vanderbilt, D. Electric Displacement as the Fundamental Variable in Electronic-Structure Calculations. *Nat. Phys.* **2009**, *5*, 304−308.
(51) McGrath, M. J.; Siepmann, J. I.; Kuo, I.-F. W.; Mundy, C. J.; VandeVondele, J.; Hutter, J.; Mohamed, F.; Krack, M. Isobaric-Isothermal Monte Carlo Simulations from First Principles: Application to Liquid Water at Ambient Conditions. *ChemPhysChem* **2005**, *6*, 1894−1901.
(52) Iftimie, R.; Salahub, D. Using a Classical Potential as an Efficient Importance Function for Sampling from an Ab Initio Potential. *Chem. Phys.* **2000**, *113*, 4852−4862.
(53) Gelb, L. D. Monte Carlo Simulations Using Sampling from an Approximate Potential. *J. Chem. Phys.* **2003**, *118*, 7747−7750.
(54) Izvekov, S.; Swanson, J. M. J. Using Force-Matching to Reveal Essential Differences between Density Functionals in Ab Initio Molecular Dynamics Simulations. *J. Chem. Phys.* **2011**, *134*, 194109.
(55) Brockwell, A. Parallel Markov Chain Monte Carlo Simulation by Pre-Fetching. *J. Comput. Graph. Stat.* **2006**, *15*, 1−18.
(56) Röttger, K.; Endriss, A.; Ihringer, J.; Doyle, S.; Kuhs, W. F. Lattice Constants and Thermal Expansion of H_2O and D_2O Ice Ih between 10 and 265 K. *Acta Crystallogr. B* **1994**, *50*, 644−648.
(57) Howe, R.; Whitworth, R. W. A Determination of the Crystal Structure of Ice XI. *J. Chem. Phys.* **1989**, *90*, 4450−4453.
(58) McDowell, S.; Amos, R.; Handy, N. Molecular Polarisabilities - A Comparison of Density Functional Theory with Standard Ab Initio Methods. *Chem. Phys. Lett.* **1995**, *235*, 1−4.